

Thermal and Transport Properties of Na[N(SO₂F)₂]-[N-methyl-N-propylpyrrolidinium][N(SO₂F)₂] Ionic Liquids
for Na Secondary Batteries

Kazuhiko Matsumoto^{}, Yu Okamoto, Toshiyuki Nohira^{*}, Rika Hagiwara*

Graduate School of Energy Science, Kyoto University, Sakyo-ku, Kyoto 606-8501, Japan

Abstract

Understanding ion transport in electrolytes is crucial for fabricating high-performance batteries. Although several ionic liquids have been explored for use as electrolytes in Na secondary batteries, little is known about the transport properties of Na⁺ ions. In this study, the thermal and transport properties of Na[FSA]-[C₃C₁pyrr][FSA] (FSA⁻: bis(fluorosulfonyl)amide and C₃C₁pyrr⁺: *N*-methyl-*N*-propylpyrrolidinium) ionic liquids were investigated in order to determine their suitability for use as electrolytes in Na secondary batteries. In the $x(\text{Na[FSA]})$ range of 0.0–0.5 ($x(\text{Na[FSA]})$ = molar fraction of Na[FSA]), a wide liquid-phase temperature range was observed at close to room temperature. The viscosity and ionic conductivity of this system, which obey the Vogel–Tamman–Fulcher equation, increases and decreases, respectively, with an increase in $x(\text{Na[FSA]})$. Further, its viscosity and molar ionic conductivity satisfy the fractional Walden rule. The apparent transport number of Na⁺ in the investigated ionic liquids, as determined by the potential step method at 353 K, increases monotonously with an increase in $x(\text{Na[FSA]})$, going from 0.08 for $x(\text{Na[FSA]}) = 0.1$ to 0.59 for $x(\text{Na[FSA]}) = 0.7$. The Na⁺ ion conductivity, determined by multiplying the ionic conductivity with the apparent transport number, is an indicator of Na⁺ ion transport in Na secondary batteries and is high when $x(\text{Na[FSA]})$ is in the 0.2–0.4 range.

Introduction

Ionic liquids have been studied intensively as electrolytes for electrochemical devices such as Li-ion batteries, electrochemical capacitors, dye-sensitized solar cells, and fuel cells.¹⁻⁴ The use of ionic liquids allows for the safety-conscious design of electrochemical devices, owing to the intrinsic properties of ionic liquids, which include low volatility, low flammability, and a wide liquid-phase temperature range.⁵ Although the required characteristics of ionic liquid electrolytes differ depending on the device in which they are to be used, a high ionic conductivity and a wide electrochemical window are generally preferred.

Ion transport in ionic liquids has been the target of extensive investigations because it governs the performance of the resultant electrochemical devices. The molar ionic conductivity (λ), which is obtained by dividing the ionic conductivity (σ) by the molar concentration ($c = \rho/FW$, where ρ and FW denote the density and the formula weight, respectively), and the viscosity (η) of neat ionic liquids are related by the Walden rule, which is represented by Equation (1)⁶⁻⁹. Thus, ionic liquids with low viscosities are generally preferred as electrolytes.

$$\lambda \cdot \eta = \text{const.} \tag{1}$$

Although a 1 M KCl aqueous solution, which exhibits a fully dissociated state, is often used as the standard,¹⁰ KCl aqueous solutions of different concentrations do not exhibit the same behavior.¹¹ For example, the behavior of the infinitely diluted KCl solution deviates from the ideal one, which is considered to result from the change in ionicity.

The ratio of diffusion coefficients of ions in ionic liquids can be determined by the pulsed-gradient spin-echo nuclear magnetic resonance technique.¹²⁻¹⁵ In shuttle-type batteries, the case is different from that of batteries based on neat ionic liquids: the transport of a specific ion (Li^+ in the case of Li secondary batteries) is the key factor in determining battery performance. The transport of such ions in the electrolyte is governed by the ionic conductivity of the electrolyte and the transport number of the

ions (t_i); the transport number is the fraction of current carried by particular ions in the electrolyte, as shown in Equation (2).

$$t_i = |z_i|c_i u_i / \sum |z_i|c_i u_i \quad (2)$$

where z_i , c_i , and u_i denote the charge number, concentration, and mobility of the particular ion, respectively.

Na secondary batteries are attracting attention for large-scale energy storage and electric vehicles, owing to the high natural abundance of Na and their low cost.¹⁶⁻¹⁸ While organic solutions containing the appropriate Na salt, such as Na[ClO₄] and Na[PF₆], are used widely in Na secondary batteries,¹⁹ there have been several recent studies on the use of ionic liquid electrolytes in these batteries.²⁰⁻²⁴ In our recent studies, we found that purely inorganic²⁵⁻²⁶ and inorganic-organic hybrid²⁷⁻²⁸ ionic liquid electrolytes based on the bis(fluorosulfonyl)amide anion (FSA⁻) exhibited good performance. The Na[FSA]-[C₃C₁pyrr][FSA] system can act as an electrolyte at temperatures of 253–363 K when used with various electrode materials,²⁷ including hard carbon,²⁹ NaCrO₂,^{27, 30} Na_{2-x}Fe_{1+2x}P₂O₇,³¹ and NaMnSiO₄.³² In particular, improvements in cycling and rate performances at elevated temperatures are observed for these electrode materials, owing to the increase in ion mobility and the electrode reaction rate. According to a previous study,²⁷ the ionic conductivity of Na[FSA]-[C₃C₁pyrr][FSA] ionic liquids decreases with an increase in the Na fraction ($x(\text{Na[FSA]})$), which corresponds to an increase in viscosity. On the other hand, the rate capability of Na/Na[FSA]-[C₃C₁pyrr][FSA]/NaCrO₂ cells is the maximum at $x(\text{Na[FSA]}) = 0.4$ in the range of $0.2 \leq x(\text{Na[FSA]}) \leq 0.6$. These results indicate clearly that the ionic conductivities of Na[FSA]-[C₃C₁pyrr][FSA] ionic liquids do not reflect the maximum of Na⁺ ion transport, and that the concentration of the Na⁺ ions should also be taken into consideration. With this in mind, we investigated the transport properties of Na⁺ ions in this ionic liquid system and attempted to optimize $x(\text{Na[FSA]})$ for Na secondary batteries.

The phase diagram of the Na[FSA]-[C₃C₁pyrr][FSA] system was constructed on the basis of the results of differential scanning calorimetry (DSC) analysis, in order to determine the optimal temperature range for its use as an electrolyte. The relationship between its viscosity and ionic conductivity is discussed based on its Walden plot. The value of $x(\text{Na[FSA]})$ optimized in terms of the Na⁺ ion conductivity is determined by measuring the transport number of Na⁺ and multiplying it by the ionic conductivity of the ionic liquid system.

Experimental section

General experimental procedure. All the volatile materials used were handled using a vacuum line constructed of SUS316 stainless steel and tetrafluoroethylene–perfluoroalkylvinylether copolymer.³³ All the nonvolatile materials were handled in a drybox in an atmosphere of dry Ar. The [C₃C₁pyrr][FSA] (Kanto Chemical Inc., purity 99.9%, water content < 39 ppm) and Na[FSA] (Mitsubishi Materials Electronic Chemicals Co., Ltd., purity 99%, water content < 72 ppm) salts were dried under vacuum at 353 K.

Analysis. The melting and glass transition temperatures were determined using a DSC system (DSC-8230, Rigaku Thermo Plus EVO II Series) at a scan rate of 5 K min⁻¹. The samples for DSC were sealed in airtight Al cells in an atmosphere of dry Ar. The viscosities of the ionic liquids were measured using a cone and plate rheometer (LV DV-II+PRO, Brookfield Engineering Laboratories, Inc.) in an atmosphere of dry air. The ionic conductivities were measured using the AC impedance technique with the aid of an impedance analyzer (3532-80, Hioki E.E. Corp.). The samples for the ionic conductivity measurements were sealed in an atmosphere of dry Ar into an airtight T-shaped cell equipped with stainless steel disk electrodes. The cell was placed in a thermostatic chamber (SU-241, ESPEC). The densities were measured using an oscillating U-tube density meter (DMA 4500 M, Anton Paar GmbH). The water contents were measured using the Karl-Fischer titration method (899 Coulometer, Metrohm).

The apparent transport number was measured using a symmetric Na/Na[FSA]-[C₃C₁pyrr][FSA]/Na coin-type cell at 353 K; a Biologic VSP-300 electrochemical measurement system was employed for the

purpose. Aluminum plates were used as the current collectors, and a glass microfiber filter (Whatman GF/A) was used as the separator which was impregnated with the electrolyte under vacuum prior to the measurement.

Results and discussion

Thermal behavior. The thermal transitions undergone by the Na[FSA]–[C₃C₁pyrr][FSA] system and determined from the results of the DSC analysis, are shown in Figure 1. The DSC data and curves are shown in Table 1 and Supporting Information (Figures S1–S10), respectively. Solid-solid transitions were observed at 193 K and 254 K for $x(\text{Na[FSA]}) = 0.0$ (Figure S1); these results agree with those reported previously.³⁴ For $x(\text{Na[FSA]})$ of 0.2–0.5, no crystallization occurred, and only glass transitions were observed during the DSC analysis. For $x(\text{Na[FSA]}) = 0.6$, as shown in Figure S7, a broad and weak endothermic peak was observed during the first heating process; this corresponded to the melting of Na[FSA]. The supercooled liquid froze at 258 K during the first cooling scan and then melted at 237 K during the second heating scan. This phenomenon is probably related to the fact that the solid phase formed during the second heating scan was different from the one formed during the initial scan, since it has been reported that Na[FSA] exhibits three polymorphs, which have different melting temperatures.³⁴ Because a white powder formed after aging at room temperature for one day in the case of the completely melted sample, the second phase was considered to be in a metastable state. A similar thermal behavior was observed for the salts with $x(\text{Na[FSA]}) = 0.7, 0.8,$ and 0.9 (Figures S8–S10). For $x(\text{Na[FSA]}) = 0.8$, two metastable states seemed to exist. An endothermic peak was observed at 272 K during the second heating process (melting of the first metastable state), while an exothermic peak appeared at 278 K (freezing of the first metastable state), followed by an endothermic peak at 283 K (melting of the second metastable state), as shown in Figure S9. Although the existence of these metastable phases makes the phase diagram look complex, it is clearly shown that the $x(\text{Na[FSA]})$ values of 0.0–0.5 are suitable for electrolytes for Na secondary batteries from the viewpoint of operation at low to intermediate temperatures.

Table 1 DSC transition temperatures ($^{\circ}\text{K}$) and changes in the enthalpy ($^{\circ}\text{kJ mol}^{-1}$) of the Na[FSA]–[C₃C₁pyrr][FSA] system^a

| $x(\text{Na[FSA]})$ | $T_{m_o}(1)$ | $T_{m_e}(1)$ | $T_{m_o}(2)$ | $T_{m_e}(2)$ | T_g | T_{tr_o} | T_{tr_e} |
|---------------------|--------------|--------------|--------------|--------------|-------|--------------------------|------------|
| 0.0 | 265 (7.7) | 273 | - | - | - | 193 (0.5) 254 (2.3) | |
| 0.1 | 231 (8.5) | 262 | - | - | - | - | - |
| 0.2 | - | - | - | - | 178 | - | - |
| 0.3 | - | - | - | - | 186 | - | - |
| 0.4 | - | - | - | - | 196 | - | - |
| 0.5 | - | - | - | - | 207 | - | - |
| 0.6 | 334 (0.5) | 368 | 237 (1.6) | 264 | 212 | - | - |
| 0.7 | 331 (0.9) | 371 | 258 (2.2) | 273 | 213 | - | - |
| 0.8 | 338 (3.1) | 373 | - | - | - | 272 (n.c.) 283 (n.c.) | 278 |
| 0.9 | 330 (7.7) | 384 | - | - | 255 | - | - |

^a $T_{m_o}(1)$ and $T_{m_e}(1)$: Melting onset and final temperatures, respectively; $T_{m_o}(2)$ and $T_{m_e}(2)$: Melting onset and final temperatures for the metastable state, respectively; T_g : glass-transition temperature; and T_{tr_o} and T_{tr_e} : Onset and final temperatures for solid-solid phase transition. The enthalpy values ($\Delta H / \text{kJ mol}^{-1}$, calculated from the peak area) are shown in parentheses. n.c.: not calculated, owing to the complicated transition behavior.

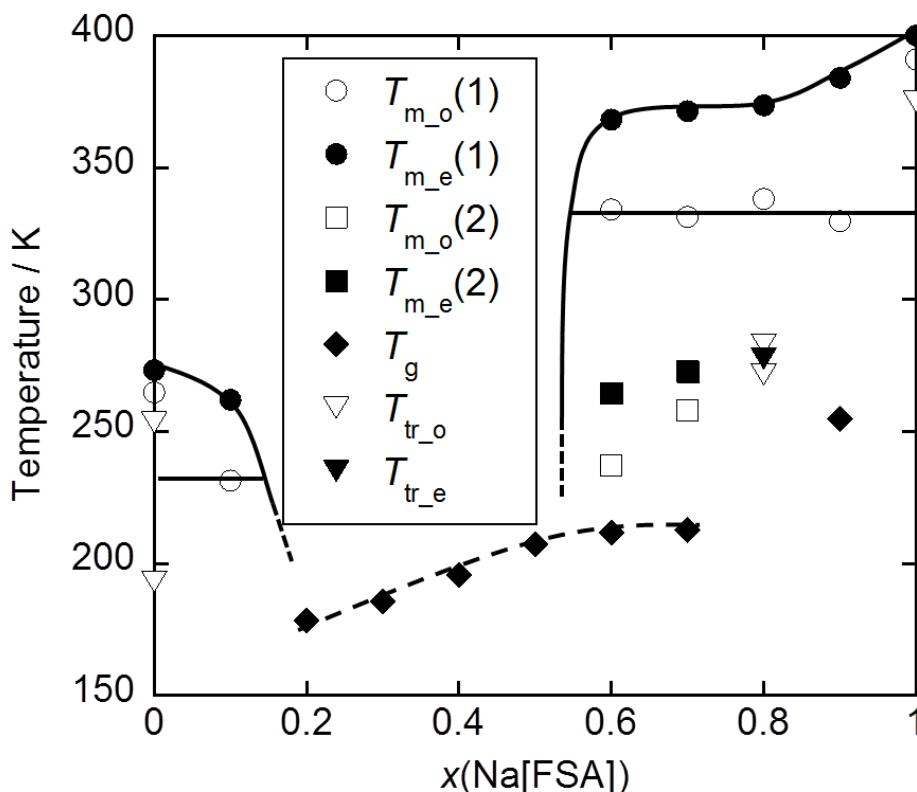


Figure 1 Phase diagram of the Na[FSA]–[C₃C₁pyrr][FSA] system. $T_{m_o}(1)$ and $T_{m_e}(1)$: Melting onset and final temperatures, respectively; $T_{m_o}(2)$ and $T_{m_e}(2)$: Melting onset and final temperatures for the metastable state, respectively; T_g : glass-transition temperature; and T_{tr_o} and T_{tr_e} : Onset and final temperatures for solid-solid phase transition.

Density, viscosity, and ionic conductivity. The temperature dependences of the density, viscosity, and ionic conductivity for the Na[FSA]-[C₃C₁pyrr][FSA] system are shown in Figures 2, 3, and 4, respectively. The densities of the Na[FSA]-[C₁C₃pyr][FSA] system are listed in Table 2. For the investigated temperature range, the density of the system increased with an increase in $x(\text{Na[FSA]})$ and decreased with an increase in the temperature, exhibiting a linear relationship, which could be represented by Equation (3) in which A and B are the fitting parameters:

$$\rho = AT + B \quad (3)$$

Table 2 Densities (g cm⁻³) of the Na[FSA]-[C₃C₁pyrr][FSA] system

| T / K | $x(\text{Na[FSA]})$ | | | | | |
|---------------------|---------------------|--------|--------|--------|--------|--------|
| | 0 | 0.1 | 0.2 | 0.3 | 0.4 | 0.5 |
| 278 | 1.3546 | 1.3844 | 1.4296 | 1.4791 | 1.5327 | 1.5962 |
| 288 | 1.3464 | 1.3761 | 1.4212 | 1.4705 | 1.5236 | 1.5868 |
| 298 | 1.3383 | 1.3679 | 1.4127 | 1.4618 | 1.5147 | 1.5775 |
| 308 | 1.3303 | 1.3597 | 1.4043 | 1.4531 | 1.5057 | 1.5681 |
| 318 | 1.3225 | 1.3516 | 1.3960 | 1.4445 | 1.4967 | 1.5591 |
| 328 | 1.3147 | 1.3437 | 1.3876 | 1.4359 | 1.4877 | 1.5501 |
| 338 | 1.3071 | 1.3359 | 1.3794 | 1.4275 | 1.4787 | 1.5411 |
| 348 | 1.2995 | 1.3281 | 1.3712 | 1.4191 | 1.4695 | 1.5323 |
| 358 | 1.2919 | 1.3204 | 1.3630 | 1.4107 | 1.4601 | 1.5235 |
| $A \times 10^4{}^a$ | -9.08 | -9.05 | -8.56 | -8.33 | -8.00 | -7.83 |
| $B{}^a$ | 1.8481 | 1.7842 | 1.7170 | 1.6610 | 1.6065 | 1.5717 |

^aThe symbols A and B are the constants in Equation (3) for the relationship expressing the temperature dependence of the density.

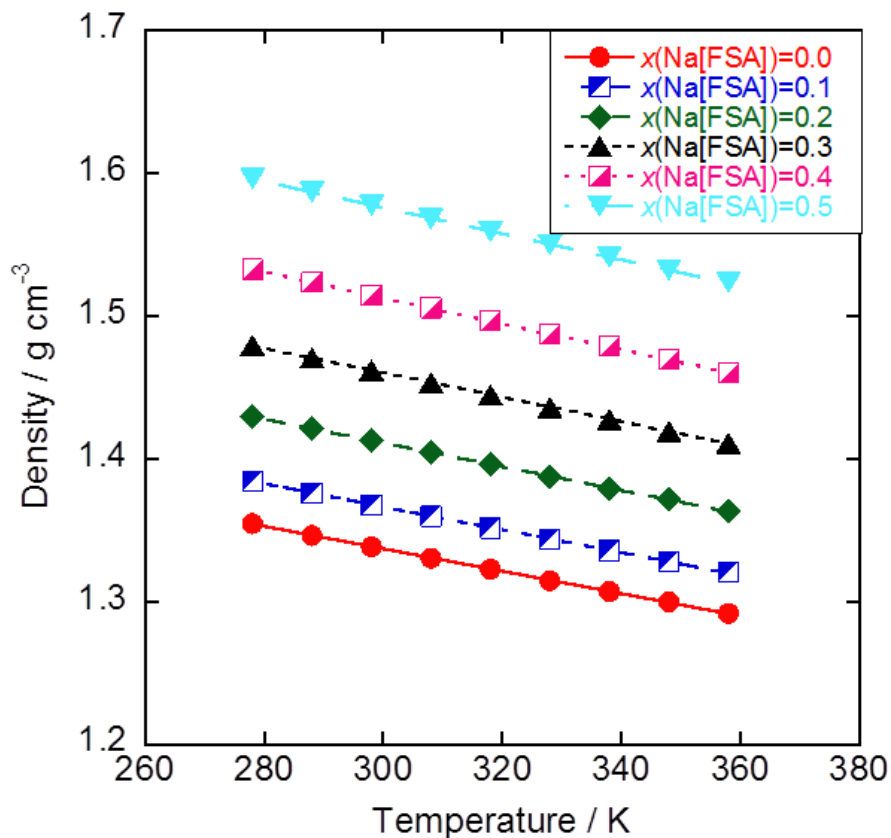


Figure 2 Temperature dependence of the densities of the Na[FSA]-[C₃C₁pyrr][FSA] ionic liquids for $x(\text{Na[FSA]})$ values of 0.0–0.5.

The molar concentration of Na[FSA] in the Na[FSA]-[C₃C₁pyrr][FSA] system was calculated from the density and formula weight and is listed in Table 3. The molar concentration is approximately 1 M at $x(\text{Na[FSA]}) = 0.2$ and approximately 3 M at $x(\text{Na[FSA]}) = 0.5$. A high Na[FSA] concentration is beneficial for improving the supply of Na⁺ ions at the electrode surface in Na secondary batteries, even though it increases the viscosity, as shown below.

Table 3 Molar concentrations of Na[FSA] in the Na[FSA]-[C₃C₁pyrr][FSA] system

| T / K | $x(\text{Na[FSA]})$ | | | | | |
|----------------|---------------------|-------|-------|-------|-------|-------|
| | 0 | 0.1 | 0.2 | 0.3 | 0.4 | 0.5 |
| 278 | 0 | 0.465 | 0.995 | 1.603 | 2.302 | 3.121 |
| 288 | 0 | 0.462 | 0.989 | 1.594 | 2.289 | 3.102 |
| 298 | 0 | 0.459 | 0.983 | 1.584 | 2.275 | 3.084 |
| 308 | 0 | 0.457 | 0.978 | 1.575 | 2.262 | 3.066 |
| 318 | 0 | 0.454 | 0.972 | 1.566 | 2.248 | 3.048 |
| 328 | 0 | 0.451 | 0.966 | 1.556 | 2.235 | 3.030 |
| 338 | 0 | 0.449 | 0.960 | 1.547 | 2.221 | 3.013 |
| 348 | 0 | 0.446 | 0.954 | 1.538 | 2.208 | 2.996 |
| 358 | 0 | 0.443 | 0.949 | 1.529 | 2.193 | 2.979 |

The viscosities and ionic conductivities of the investigated system are listed in Tables 4 and 5, respectively. The Arrhenius plots of the viscosity and ionic conductivity are concave and convex curves, respectively, and obey the Vogel-Tamman-Fulcher (VTF) equation³⁵⁻³⁶ (Equations (4) and (5), with A_η , B_η , $T_{0\eta}$, A_σ , B_σ , and $T_{0\sigma}$ being the fitting parameters ($R^2 > 0.999$, see Tables S1 and S2)), instead of the Arrhenius equation. This is in keeping with previous reports on neat ionic liquids:^{9, 12-13}

$$\eta(T) = A_\eta T^{1/2} \exp\left(\frac{B_\eta}{T - T_{0\eta}}\right) \quad (4)$$

$$\sigma(T) = A_\sigma T^{-1/2} \exp\left(-\frac{B_\sigma}{T - T_{0\sigma}}\right) \quad (5)$$

The parameters B_η and B_σ , which are related to the activation energies, increased with an increase in $x(\text{Na}[\text{FSA}])$; this is reflected in the gradients of the plots in the high-temperature range. T_0 is the "ideal glass-transition temperature," and is usually lower than the glass-transition temperature observed during the DSC measurements.²

Table 4 Viscosities (mPa s) of the Na[FSA]-[C₃C₁pyrr][FSA] system

| T / K | $x(\text{Na}[\text{FSA}])$ | | | | | | | |
|----------------|----------------------------|-----|-----|-----|------|------|------|------|
| | 0.0 | 0.1 | 0.2 | 0.3 | 0.4 | 0.5 | 0.6 | 0.7 |
| 278 | 90 | 145 | 274 | 548 | 1178 | - | - | - |
| 288 | 60 | 90 | 153 | 28 | 578 | 1746 | - | - |
| 298 | 41 | 60 | 95 | 163 | 303 | 779 | - | - |
| 308 | 30 | 42 | 63 | 100 | 177 | 385 | 1217 | - |
| 318 | 22 | 30 | 43 | 64 | 107 | 222 | 538 | 1360 |
| 328 | 17 | 22 | 31 | 44 | 70 | 131 | 34 | 658 |
| 338 | 13 | 17 | 23 | 32 | 49 | 85 | 179 | 360 |
| 348 | 11 | 14 | 18 | 23 | 35 | 56 | 117 | 216 |

Table 5 Ionic conductivities (mS cm^{-1}) of the $\text{Na[FSA]}-[\text{C}_3\text{C}_1\text{pyrr}][\text{FSA}]$ system

| T / K | $x(\text{Na[FSA]})$ | | | | | | | |
|----------------|---------------------|------|------|------|------|------|------|------|
| | 0.0 | 0.1 | 0.2 | 0.3 | 0.4 | 0.5 | 0.6 | 0.7 |
| 248 | - | - | 0.17 | 0.06 | - | - | - | - |
| 258 | 1.6 | 0.86 | 0.40 | 0.15 | 0.04 | - | - | - |
| 268 | 2.7 | 1.5 | 0.80 | 0.35 | 0.11 | 0.03 | - | - |
| 278 | 4.1 | 2.5 | 1.4 | 0.71 | 0.26 | 0.10 | 0.02 | - |
| 288 | 6.0 | 3.9 | 2.4 | 1.1 | 0.56 | 0.24 | 0.08 | 0.02 |
| 298 | 8.0 | 5.5 | 3.6 | 1.9 | 1.0 | 0.51 | 0.20 | 0.06 |
| 308 | 10.6 | 7.5 | 5.1 | 3.0 | 1.8 | 0.94 | 0.43 | 0.16 |
| 318 | 13.6 | 10.0 | 7.0 | 4.5 | 2.8 | 1.6 | 0.85 | 0.36 |
| 328 | 16.9 | 12.9 | 9.3 | 6.5 | 4.1 | 2.6 | 1.5 | 0.73 |
| 338 | 20.4 | 16.0 | 11.9 | 8.9 | 5.6 | 3.8 | 2.5 | 1.3 |
| 348 | 24.4 | 19.4 | 14.8 | 11.2 | 7.9 | 5.4 | 3.8 | 2.2 |
| 358 | 28.7 | 23.4 | 18.1 | 14.1 | 10.3 | 7.4 | 5.5 | 3.5 |
| 368 | 33.2 | 27.3 | 21.4 | 17.3 | 12.9 | 9.7 | 7.5 | 5.2 |

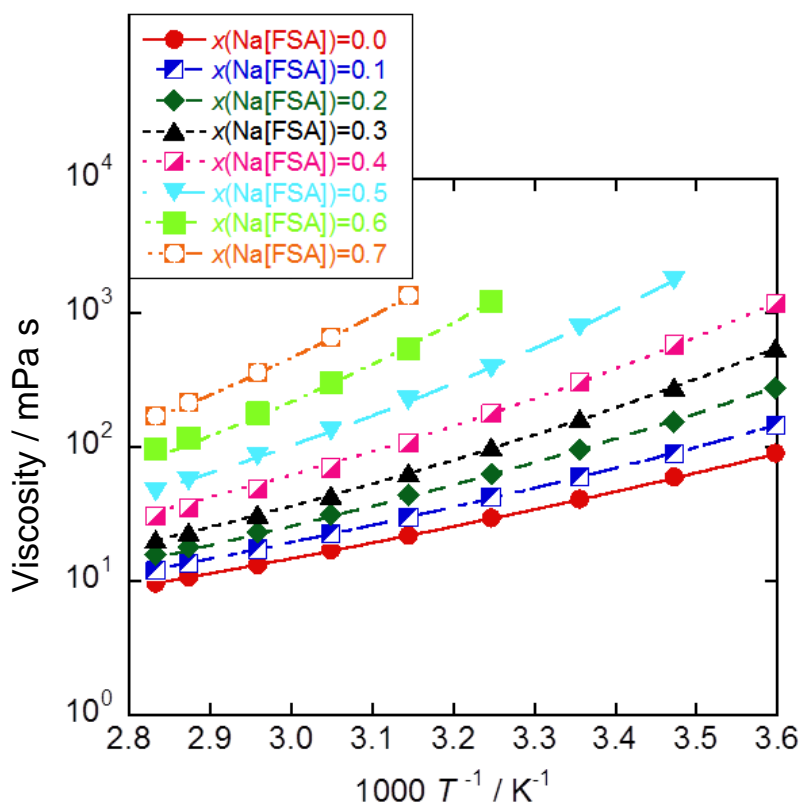


Figure 3 Arrhenius plots of the viscosities of the $\text{Na[FSA]}-[\text{C}_3\text{C}_1\text{pyrr}][\text{FSA}]$ ionic liquids for $x(\text{Na[FSA]})$ values of 0.0–0.7.

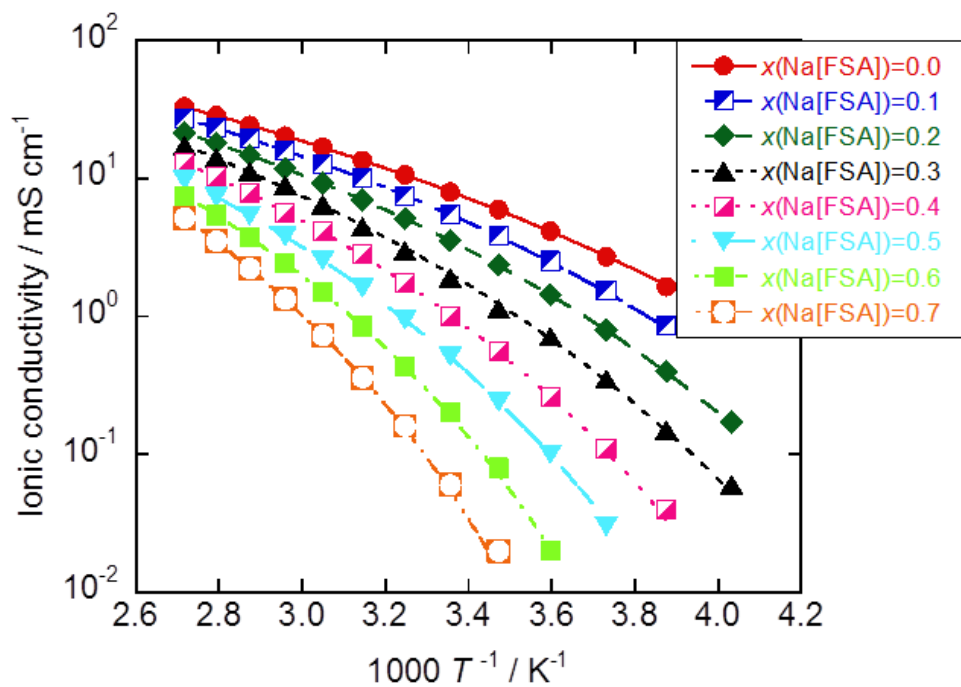


Figure 4 Arrhenius plots of the ionic conductivities of the Na[FSA]–[C₃C₁pyrr][FSA] ionic liquids for $x(\text{Na[FSA]})$ values of 0.0–0.7.

The plots of the logarithm of the molar conductivity against the logarithm of the reciprocal of the viscosity (i.e., the Walden plots) for the Na[FSA]–[C₃C₁pyrr][FSA] ionic liquids are shown in Figure 5. If an electrolyte obeys the Walden rule, the product of its molar conductivity and viscosity is constant, as can be seen from Equation (1). The ionic conductivities of the Na[FSA]–[C₃C₁pyrr][FSA] ionic liquids were lower than those expected from their viscosities based on the Walden rule. As in the case with most ionic liquids, this behavior suggests there is a high degree of correlation between the motion of the cations and anions.³⁷ By carefully looking at the Walden plots for this system, one can notice that their gradients are smaller than unity. In such cases, the relationship between the molar conductivity and the viscosity can be described by the fractional Walden rule, which can be expressed by Equation (6):^{9,37}

$$\lambda \cdot \eta^\alpha = \text{const.} \tag{6}$$

where α is called the decoupling constant, ranges from zero to unity, and corresponds to the slope of the Walden plot. It has been reported that the parameter α is independent of the temperature and pressure.³⁸ For the Na[FSA]–[C₃C₁pyrr][FSA] ionic liquids, the values of α ranged from 0.85 to 0.97 (0.85 for $x(\text{Na[FSA]}) = 0.0$, 0.88 for $x(\text{Na[FSA]}) = 0.1$, 0.87 for $x(\text{Na[FSA]}) = 0.2$, 0.91 for $x(\text{Na[FSA]}) = 0.3$, 0.97 for $x(\text{Na[FSA]}) = 0.4$, and 0.92 for $x(\text{Na[FSA]}) = 0.5$); these values are very similar to those reported previously for neat ionic liquids (e.g., 0.90–0.94 for a few imidazolium-based ionic liquids¹¹). Although this is not completely evident from the results of the present study, it is likely that α increases with an increase in $x(\text{Na[FSA]})$, that is, the relation between λ and η can be approximated by the Walden rule (Equation (1)). The parameter α also reflects the ratio of the B parameters of the ionic conductivity (B_σ) and the viscosity (B_η);³⁹ however, the physical meaning of B_σ and B_η in the VTF equation depends on the theoretical interpretations of Equations (4) and (5).⁹

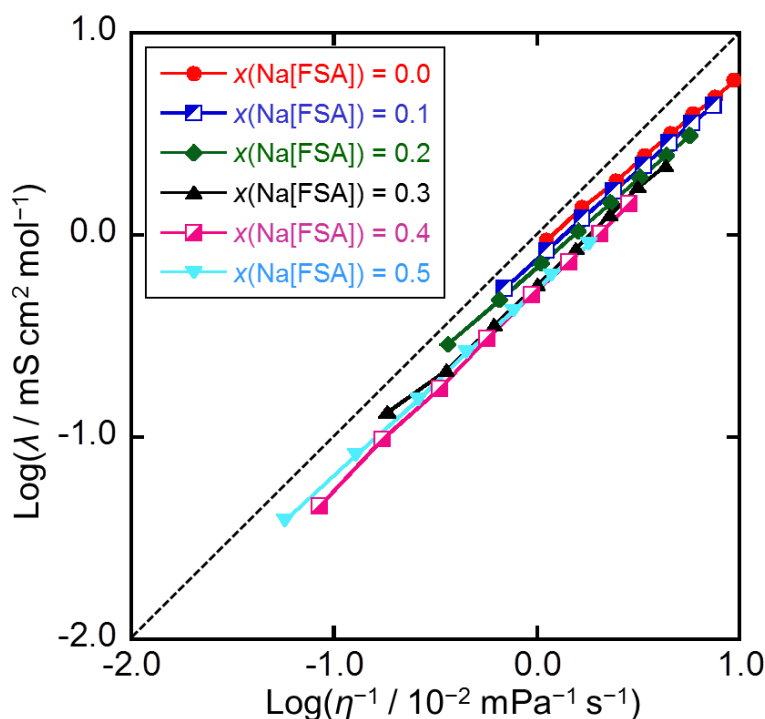


Figure 5 Walden plots for the Na[FSA]–[C₃C₁pyrr][FSA] ionic liquids for $x(\text{Na[FSA]})$ values of 0.0–0.5. The dashed line is a visual guide representing $\alpha = 1$ in Equation (6).

Apparent transport number. The transport number of Na⁺ in the Na[FSA]–[C₃C₁pyrr][FSA] ionic liquids was estimated using a previously reported AC-DC method.⁴⁰⁻⁴¹ A Na/Na[FSA]–

[C₁C₃pyr][FSA]/Na two-electrode cell was used at 353 K for the purpose; the separator thickness was 0.52 mm. A temperature of 353 K was chosen by considering previous reports on Na secondary batteries using this ionic liquid as the electrolyte.³⁰ The bulk resistance (R_b^0) and charge-transfer resistance (R_e^0) in the initial state were measured by the AC impedance method using a two-electrode cell. Then, a cell voltage of 10 mV (ΔV) was applied to measure the initial current (I^0) and the steady-state current (I^s) during polarization. The current stabilized after 8 h for all $x(\text{Na}[\text{FSA}])$ values; the steady state can be expressed by the following Equation (7):



Finally, an AC impedance measurement was made to determine the bulk resistance (R_b^s) and the charge-transfer resistance (R_e^s) for the steady state. It should be noted that the transport number obtained for the Na[FSA]–[C₃C₁pyrr][FSA] system using this method might be different from that for electrolytes in a solvent or polymer matrix; this would be owing to the difference in the environment of the ions in the initial and steady states. When considering the ions in a solvent (or a polymer) in the case of shuttle-type (cation shuttle) secondary batteries, both cations and anions move in the solvent in the initial state, while only the cations move in the steady state. The environments of the cations in both the states are similar, because the cations are surrounded by the solvent, which acts as a fixed matrix. On the other hand, for the Na[FSA]–[C₃C₁pyrr][FSA] system, in the steady state, the cations could have a totally different environment from that in the initial state, because there is no fixed matrix. As a result, the mobility of Na⁺ ions in the steady state ($u'(\text{Na}^+)$) would be different from that in the initial state ($u(\text{Na}^+)$). Taking into account this difference, the transport number obtained in this study is termed the "apparent transport number (t').". The reason " t' " derived using the AC-DC method is used is that the Na⁺ ion conductivity determined from t' (see below) can be used to evaluate Na⁺ ion transport in the Na[FSA]–[C₃C₁pyrr][FSA] ionic liquids. The apparent transport number of Na⁺ ($t'(\text{Na}^+)$) could be represented by Equation (8) and was determined by substituting the variables in Equation (9) with the measured values:

$$t'(\text{Na}^+) = \frac{x(\text{Na}[\text{FSA}]) \times u'(\text{Na}^+)}{x(\text{Na}[\text{FSA}]) \times u(\text{Na}^+) + (1 - x(\text{Na}[\text{FSA}])) \times u(\text{C}_3\text{C}_1\text{pyrr}^+) + u(\text{FSA}^-)} \quad (8)$$

$$t'(\text{Na}^+) = \frac{I^s \times R_b^s \times (\Delta V - I^0 \times R_e^0)}{I^0 \times R_b^0 \times (\Delta V - I^s \times R_e^s)} \quad (9)$$

where $u(\text{C}_3\text{C}_1\text{pyrr}^+)$ and $u(\text{FSA}^-)$ are the mobilities of $\text{C}_3\text{C}_1\text{pyrr}^+$ and FSA^- ions in the initial state.

The Nyquist plot (200 kHz to 1 Hz) and time dependence of the current during polarization for $x(\text{Na}[\text{FSA}]) = 0.2$ obtained at 353 K are shown in Figures 6 (a) and (b), respectively (see Figures S11–S16 for the chronoamperograms and Nyquist plots corresponding to the other $x(\text{Na}[\text{FSA}])$ values). The other parameters related to the transport properties of Na^+ ions are listed in Table 6. The relationship between $x(\text{Na}[\text{FSA}])$ and $t'(\text{Na}^+)$ at 353 K is shown in Figure 7. The $t'(\text{Na}^+)$ value increased monotonously with the increase in $x(\text{Na}[\text{FSA}])$. Although it is not fully clear from this result, the gradient of this relationship may change for $x(\text{Na}[\text{FSA}]) > 0.5$. In a previous study on the [DEME][TFSA]-Li[TFSA] system (DEME: *N,N*-diethyl-*N*-methyl-*N*-2-methoxyethylammonium and TFSA: bis(trifluoromethylsulfonyl)amide), the apparent transport number of Li^+ was determined to be 0.13 using the same method; this was for a Li[TFSA] molar fraction ($x(\text{Li}[\text{TFSA}])$) of 0.13, which corresponded to a Li[TFSA] concentration of 0.32 mol kg⁻¹.⁴² In the present Na-based system, the transport number was smaller than $x(\text{Na}[\text{FSA}])$ (the average of seven $t'(\text{Na}^+)/x(\text{Na}[\text{FSA}])$ values was 0.75). The differences in the transport properties of Li^+ and Na^+ ions, which may be owing to the effects of counteranions and the coexistent organic cations, cause this difference. The effects of the separator thickness on $t'(\text{Na}^+)$ were also investigated using the case with $x(\text{Na}[\text{FSA}]) = 0.2$ as an example. This is because the separator thickness represents the thickness of the electrolyte layer. However, the results suggested that $t'(\text{Na}^+)$ remained nearly constant irrespective of the separator thickness (0.52 mm, 0.78 mm, and 1.04 mm). An attempt to determine $t'(\text{Na}^+)$ at ambient temperatures failed, owing to the high charge-transfer resistance of the Na metal electrode.³¹

Table 6 Parameters used for determining $t'(\text{Na}^+)$ for the Na[FSA]–[C₃C₁pyrr][FSA] system and the $t'(\text{Na}^+)$ and $\sigma(\text{Na}^+)$ values at 353 K^a

| $x(\text{Na}[\text{FSA}])$ | I^0 / mA | I^s / mA | R_b^0 / Ω | R_b^s / Ω | R_e^0 / Ω | R_e^s / Ω | $t'(\text{Na}^+)$ | $\sigma(\text{Na}^+)$ |
|----------------------------|-------------------|-------------------|------------------|------------------|------------------|------------------|-------------------|-----------------------|
| 0.1 | 0.925 | 0.218 | 1.56 | 1.47 | 7.90 | 10.94 | 0.08 | 1.7 |
| 0.2 | 0.478 | 0.191 | 2.50 | 2.31 | 15.39 | 22.41 | 0.17 | 2.8 |
| 0.3 | 0.483 | 0.191 | 2.82 | 2.41 | 14.27 | 25.62 | 0.21 | 2.6 |
| 0.4 | 0.314 | 0.200 | 3.26 | 3.04 | 23.39 | 21.79 | 0.28 | 2.5 |
| 0.5 | 0.484 | 0.298 | 4.82 | 4.88 | 14.52 | 14.70 | 0.33 | 2.1 |
| 0.6 | 0.654 | 0.411 | 6.23 | 6.03 | 8.19 | 8.05 | 0.42 | 1.9 |
| 0.7 | 0.659 | 0.427 | 9.37 | 9.41 | 4.39 | 5.22 | 0.59 | 1.6 |

^a I^0 : Initial current, I^s : steady state current, R_b^0 : bulk resistance in the initial state, R_b^s : bulk resistance in the steady state, R_e^0 : charge-transfer resistance in the initial state, R_e^s : charge-transfer resistance in the steady state, and $t'(\text{Na}^+)$: apparent transport number of Na⁺.

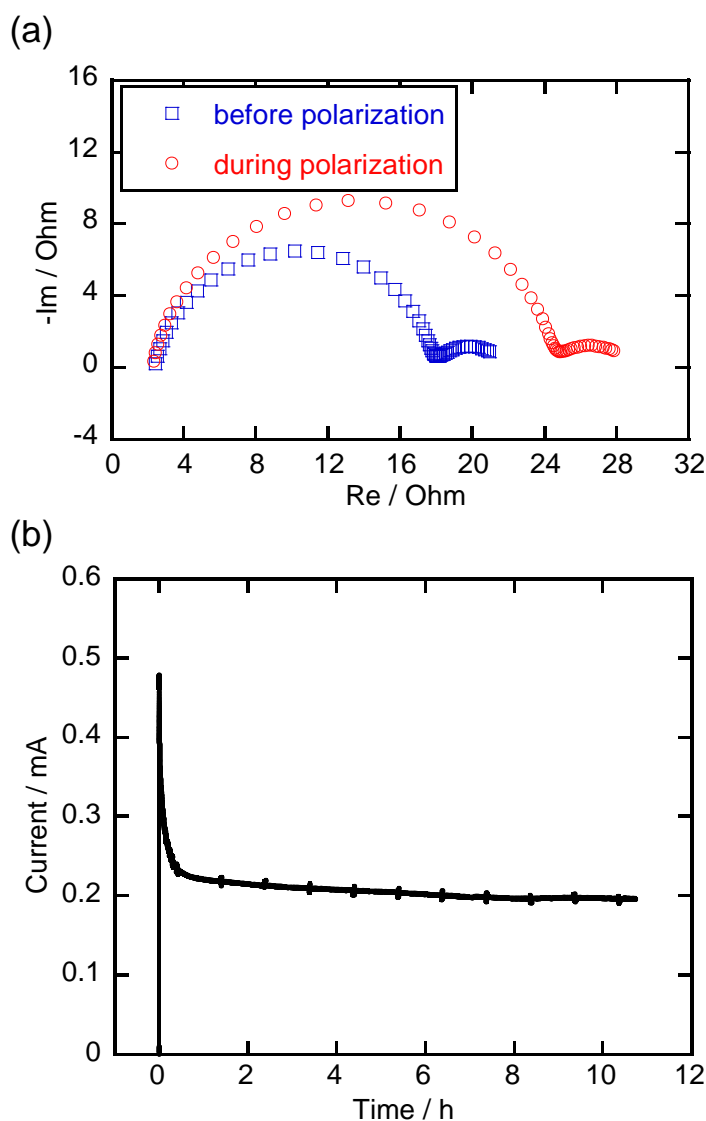


Figure 6 (a) Nyquist plot (200 kHz to 1 Hz) of the Na/Na[FSA]–[C₃C₁pyrr][FSA]/Na cell ($x(\text{Na}[\text{FSA}]) = 0.2$) at 353 K. (b) Time dependence of the current during polarization for the Na/Na[FSA]–[C₃C₁pyrr][FSA]/Na cell ($x(\text{Na}[\text{FSA}]) = 0.2$) at 353 K. Applied voltage: 10 mV.

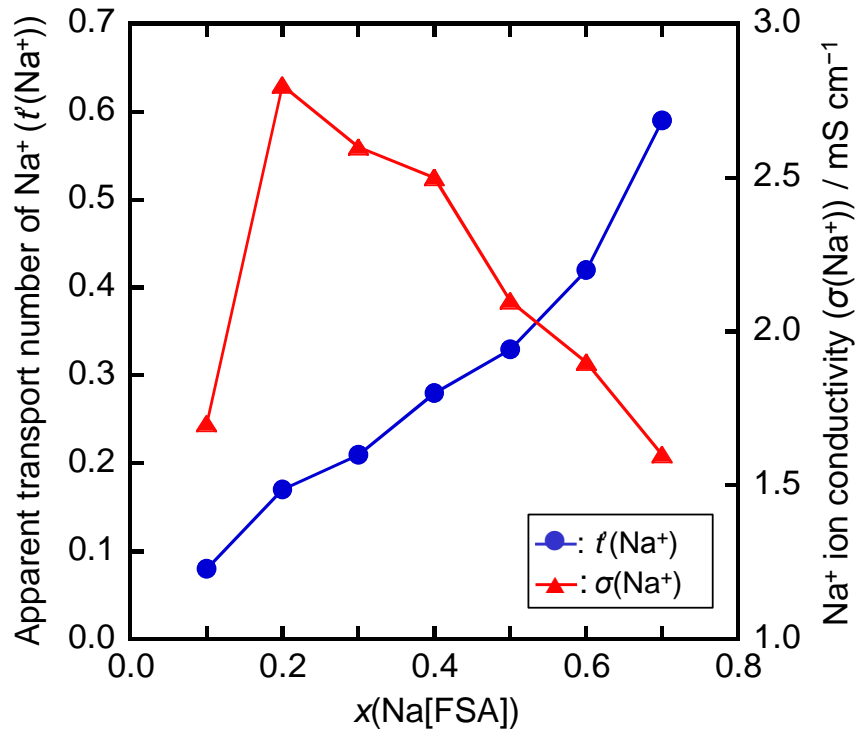


Figure 7 The $x(\text{Na[FSA]})-t'(\text{Na}^+)$ and $x(\text{Na[FSA]})-\sigma(\text{Na}^+)$ relationships for the Na/Na[FSA]-[C₃C₁pyrr][FSA]/Na cell, as determined at 353 K.

Sodium ion conductivity. The sodium ion conductivity ($\sigma(\text{Na}^+)$) can be used as a practical indicator of Na^+ transport in the electrolyte and is important for optimizing the $x(\text{Na[FSA]})$ value for electrolytes for Na secondary batteries. The $\sigma(\text{Na}^+)$ values at 353 K shown in Table 6 were calculated by multiplying the ionic conductivity of the ionic liquid ($\sigma(\text{IL})$) and $t'(\text{Na}^+)$ as per Equation (10) ($\sigma(\text{IL})$ at 353 K was calculated from the VTF equation (Equation (5) and Table S2)):

$$\sigma(\text{Na}^+) = \sigma(\text{IL}) \cdot t'(\text{Na}^+) \quad (10)$$

The obtained $\sigma(\text{Na}^+)$ values were high for $x(\text{Na[FSA]}) = 0.2, 0.3,$ and 0.4 . The $\sigma(\text{IL})$ and $t'(\text{Na}^+)$ values decreased and increased, respectively, as $x(\text{Na[FSA]})$ increased (Figure 7). These results show clearly that too high a Na^+ concentration causes an increase in viscosity and a decrease in ionic conductivity, leading to low Na ion conductivity even if the electrolyte contains a large number of Na^+

ions. In actual batteries, both a deficiency and an excess of Na^+ ions can occur near the electrodes during the charge-discharge process at high rates. Optimizing the $x(\text{Na}[\text{FSA}])$ value will aid the fabrication of high-performance Na secondary batteries.

Conclusions

In this study, the thermal and transport properties of the $\text{Na}[\text{FSA}]-[\text{C}_3\text{C}_1\text{pyrr}][\text{FSA}]$ binary system were investigated with the view of using it in Na secondary batteries. The phase diagram for the system was constructed based on the results of a DSC analysis; it showed that there exists a wide liquid-phase temperature range for $x(\text{Na}[\text{FSA}])$ values of 0–0.5. The basic physical properties of this system (i.e., the density, viscosity, and ionic conductivity) were measured. Further, it was confirmed that the fractional Walden rule applies to this system. The apparent transport number of Na^+ ($t'(\text{Na}^+)$) was obtained from the ratio of the initial and steady-state currents using the potential step method. It was found that the $t'(\text{Na}^+)$ value increased with an increase in $x(\text{Na}[\text{FSA}])$. The Na^+ ion conductivity was determined by multiplying the ionic conductivity of the ionic liquid and $t'(\text{Na}^+)$, which was high for $x(\text{Na}[\text{FSA}]) = 0.2, 0.3, \text{ and } 0.4$. In terms of Na^+ transport, optimizing the $\text{Na}[\text{FSA}]$ concentration is important for ensuring desirable charge-discharge properties at high rates.

ASSOCIATED CONTENT

Supporting Information

VTF fitting parameters, DSC curves, and electrochemical data used for determining the apparent transport number. This material is available free of charge via the Internet at <http://pubs.acs.org>.

AUTHOR INFORMATION

Corresponding Author

*E-mail: k-matsumoto@energy.kyoto-u.ac.jp (Kazuhiko Matsumoto), nohira.toshiyuki.8r@kyoto-u.ac.jp (Toshiyuki Nohira), Tel.: +81757534817

Present Addresses

Toshiyuki Nohira: Institute of Advanced Energy, Kyoto University, Uji 611-0011, Japan

Notes

The authors declare no competing financial interest.

ACKNOWLEDGMENT

This study was partly supported by the Advanced Low Carbon Technology Research and Development Program (ALCA, No. 3428) of Japan Science and Technology Agency (JST), and “Elements Strategy Initiative to Form Core Research Center” program of the Japanese Ministry of Education, Culture, Sports, Science and Technology (MEXT).

REFERENCES

- (1) Lewandowski, A.; Swiderska-Mocek, A. Ionic Liquids as Electrolytes for Li-Ion Batteries-An Overview of Electrochemical Studies. *J. Power Sources* **2009**, *194*, 601-609.
- (2) Ohno, H., *Electrochemical Aspects of Ionic Liquids*. 2nd ed.; John Wiley & Sons Inc.: Hoboken, New Jersey, 2011.
- (3) Armand, M.; Endres, F.; MacFarlane, D. R.; Ohno, H.; Scrosati, B. Ionic-Liquid Materials for The Electrochemical Challenges of the Future. *Nat. Mater.* **2009**, *8*, 621-629.
- (4) MacFarlane, D. R.; Tachikawa, N.; Forsyth, M.; Pringle, J. M.; Howlett, P. C.; Elliott, G. D.; Davis, J. H.; Watanabe, M.; Simon, P.; Angell, C. A. Energy Applications of Ionic Liquids. *Energy Environ. Sci.* **2014**, *7*, 232-250.
- (5) Hallett, J. P.; Welton, T. Room-Temperature Ionic Liquids: Solvents for Synthesis and Catalysis. 2. *Chem. Rev.* **2011**, *111*, 3508-3576.
- (6) Walden, P.; Ulich, H.; Busch, G. Conductivity Measurements in Acetone. *Z. Phys. Chem.* **1926**, *123*, 429-434.
- (7) Hagiwara, R.; Matsumoto, K.; Nakamori, Y.; Tsuda, T.; Ito, Y.; Matsumoto, H.; Momota, K. Physicochemical Properties of 1,3-Dialkylimidazolium Fluorohydrogenate Room-Temperature Molten Salts. *J. Electrochem. Soc.* **2003**, *150*, D195-D199.
- (8) Yoshida, Y.; Muroi, K.; Otsuka, A.; Saito, G.; Takahashi, M.; Yoko, T. 1-Ethyl-3-Methylimidazolium Based Ionic Liquids Containing Cyano Groups: Synthesis, Characterization, and Crystal Structure. *Inorg. Chem.* **2004**, *43*, 1458-1462.
- (9) Xu, W.; Cooper, E. I.; Angell, C. A. Ionic Liquids: Ion Mobilities, Glass Temperatures, and Fragilities. *J. Phys. Chem. B* **2003**, *107*, 6170-6178.
- (10) Xu, W.; Angell, C. A. Solvent-Free Electrolytes with Aqueous Solution - Like Conductivities. *Science* **2003**, *302*, 422-425.

- (11) Schreiner, C.; Zugmann, S.; Hartl, R.; Gores, H. J. Fractional Walden Rule for Ionic Liquids: Examples from Recent Measurements and a Critique of the So-Called Ideal KCl Line for The Walden Plot. *J. Chem. Eng. Data* **2010**, *55*, 1784-1788.
- (12) Noda, A.; Hayamizu, K.; Watanabe, M. Pulsed-Gradient Spin-Echo H^1 And F^{19} NMR Ionic Diffusion Coefficient, Viscosity, and Ionic Conductivity of Non-Chloroaluminate Room-Temperature Ionic Liquids. *J. Phys. Chem. B* **2001**, *105*, 4603–4610.
- (13) Tokuda, H.; Hayamizu, K.; Ishii, K.; Abu Bin Hasan Susan, M.; Watanabe, M. Physicochemical Properties and Structures of Room Temperature Ionic Liquids. 1. Variation of Anionic Species. *J. Phys. Chem. B* **2004**, *108*, 16593-16600.
- (14) Tokuda, H.; Hayamizu, K.; Ishii, K.; Susan, M.; Watanabe, M. Physicochemical Properties and Structures of Room Temperature Ionic Liquids. 2. Variation of Alkyl Chain Length in Imidazolium Cation. *J. Phys. Chem. B* **2005**, *109*, 6103-6110.
- (15) Tokuda, H.; Ishii, K.; Susan, M.; Tsuzuki, S.; Hayamizu, K.; Watanabe, M. Physicochemical Properties and Structures of Room-Temperature Ionic Liquids. 3. Variation of Cationic Structures. *J. Phys. Chem. B* **2006**, *110*, 2833-2839.
- (16) Pan, H. L.; Hu, Y. S.; Chen, L. Q. Room-Temperature Stationary Sodium-Ion Batteries for Large-Scale Electric Energy Storage. *Energy Environ. Sci.* **2013**, *6*, 2338-2360.
- (17) Ponrouch, A.; Dedryvere, R.; Monti, D.; Demet, A. E.; Mba, J. M. A.; Croguennec, L.; Masquelier, C.; Johansson, P.; Palacin, M. R. Towards High Energy Density Sodium Ion Batteries through Electrolyte Optimization. *Energy Environ. Sci.* **2013**, *6*, 2361-2369.
- (18) Hong, S. Y.; Kim, Y.; Park, Y.; Choi, A.; Choi, N. S.; Lee, K. T. Charge Carriers in Rechargeable Batteries: Na Ions vs. Li Ions. *Energy Environ. Sci.* **2013**, *6*, 2067-2081.
- (19) Kuratani, K.; Uemura, N.; Senoh, H.; Takeshita, H. T.; Kiyobayashi, T. Conductivity, Viscosity And Density of $MClO_4$ ($M = Li$ And Na) Dissolved in Propylene Carbonate and Gamma-Butyrolactone at High Concentrations. *J. Power Sources* **2013**, *223*, 175-182.

- (20) Monti, D.; Jonsson, E.; Palacin, M. R.; Johansson, P. Ionic Liquid Based Electrolytes for Sodium-Ion Batteries: Na⁺ Solvation and Ionic Conductivity. *J. Power Sources* **2014**, *245*, 630-636.
- (21) Noor, S. A. M.; Howlett, P. C.; MacFarlane, D. R.; Forsyth, M. Properties of Sodium-Based Ionic Liquid Electrolytes for Sodium Secondary Battery Applications. *Electrochim. Acta* **2013**, *114*, 766-771.
- (22) Kim, S. W.; Seo, D. H.; Ma, X. H.; Ceder, G.; Kang, K. Electrode Materials for Rechargeable Sodium-Ion Batteries: Potential Alternatives to Current Lithium-Ion Batteries. *Adv. Energy. Mater.* **2012**, *2*, 710-721.
- (23) Palomares, V.; Casas-Cabanas, M.; Castillo-Martinez, E.; Han, M. H.; Rojo, T. Update on Na-Based Battery Materials. A Growing Research Path. *Energy Environ. Sci.* **2013**, *6*, 2312-2337.
- (24) Wang, C.-H.; Yeh, Y.-W.; Wongittharom, N.; Wang, Y.-C.; Tseng, C.-J.; Lee, S.-W.; Chang, W.-S.; Chang, J.-K. Rechargeable Na/Na_{0.44}MnO₂ Cells with Ionic Liquid Electrolytes Containing Various Sodium Solutes. *J. Power Sources* **2015**, *274*, 1016-1023.
- (25) Fukunaga, A.; Nohira, T.; Kozawa, Y.; Hagiwara, R.; Sakai, S.; Nitta, K.; Inazawa, S. Intermediate-Temperature Ionic Liquid NaFSA-KFSA and Its Application to Sodium Secondary Batteries. *J. Power Sources* **2012**, *209*, 52-56.
- (26) Chen, C. Y.; Matsumoto, K.; Nohira, T.; Hagiwara, R.; Fukunaga, A.; Sakai, S.; Nitta, K.; Inazawa, S. Electrochemical and Structural Investigation of NaCrO₂ As A Positive Electrode for Sodium Secondary Battery Using Inorganic Ionic Liquid NaFSA-KFSA. *J. Power Sources* **2013**, *237*, 52-57.
- (27) Ding, C. S.; Nohira, T.; Hagiwara, R.; Matsumoto, K.; Okamoto, Y.; Fukunaga, A.; Sakai, S.; Nitta, K.; Inazawa, S. Na[FSA]-[C₃C₁pyrr][FSA] Ionic Liquids as Electrolytes for Sodium Secondary Batteries: Effects of Na Ion Concentration and Operation Temperature. *J. Power Sources* **2014**, *269*, 124-128.
- (28) Matsumoto, K.; Hosokawa, T.; Nohira, T.; Hagiwara, R.; Fukunaga, A.; Numata, K.; Itani, E.; Sakai, S.; Nitta, K.; Inazawa, S. The Na[FSA]-[C₂C₁im][FSA] (C₂C₁im⁺:1-Ethyl-3-Methylimidazolium and FSA⁻:Bis(fluorosulfonyl)amide) Ionic Liquid Electrolytes for Sodium Secondary Batteries. *J. Power Sources* **2014**, *265*, 36-39.

- (29) Fukunaga, A.; Nohira, T.; Hagiwara, R.; Numata, K.; Itani, E.; Sakai, S.; Nitta, K.; Inazawa, S. A Safe and High-Rate Negative Electrode for Sodium-Ion Batteries: Hard Carbon in NaFSA-C₁C₃PyrFSA Ionic Liquid at 363 K. *J. Power Sources* **2014**, *246*, 387-391.
- (30) Ding, C. S.; Nohira, T.; Kuroda, K.; Hagiwara, R.; Fukunaga, A.; Sakai, S.; Nitta, K.; Inazawa, S. NaFSA-C₁C₃PyrFSA Ionic Liquids for Sodium Secondary Battery Operating over a Wide Temperature Range. *J. Power Sources* **2013**, *238*, 296-300.
- (31) Chen, C. Y.; Matsumoto, K.; Nohira, T.; Ding, C. S.; Yamamoto, T.; Hagiwara, R. Charge-Discharge Behavior of a Na₂FeP₂O₇ Positive Electrode in an Ionic Liquid Electrolyte between 253 and 363 K. *Electrochim. Acta* **2014**, *133*, 583-588.
- (32) Chen, C. Y.; Matsumoto, K.; Nohira, T.; Hagiwara, R. Na₂MnSiO₄ as a Positive Electrode Material for Sodium Secondary Batteries Using an Ionic Liquid Electrolyte. *Electrochem. Commun.* **2014**, *45*, 63-66.
- (33) Matsumoto, K.; Hagiwara, R. Elimination of AsF₃ from Anhydrous HF Using AgFAsF₆ As a Mediator. *J. Fluorine Chem.* **2011**, *131*, 805-808.
- (34) Matsumoto, K.; Oka, T.; Nohira, T.; Hagiwara, R. Polymorphism of Alkali Bis(fluorosulfonyl)amides (M[N(SO₂F)₂], M = Na, K, And Cs). *Inorg. Chem.* **2013**, *52*, 568-576.
- (35) Vogel, H. The Temperature Dependence Law of the Viscosity of Fluids. *Phys. Z.* **1921**, *22*, 645-646.
- (36) Fulcher, G. S. Analysis of Recent Measurements of the Viscosity of Glasses. *J. Am. Ceram. Soc.* **1925**, *8*, 339-355.
- (37) Harris, K. R. Relations between The Fractional Stokes-Einstein and Nernst-Einstein Equations and Velocity Correlation Coefficients in Ionic Liquids and Molten Salts. *J. Phys. Chem. B* **2010**, *114*, 9572-9577.
- (38) Harris, K. R.; Kanakubo, M.; Tsuchihashi, N.; Ibuki, K.; Ueno, M. Effect of Pressure on the Transport Properties of Ionic Liquids: 1-Alkyl-3-Methylimidazolium Salts. *J. Phys. Chem. B* **2008**, *112*, 9830-9840.

- (39) Nitta, K.; Nohira, T.; Hagiwara, R.; Majima, M.; Inazawa, S. Physicochemical Properties of ZnCl₂-NaCl-KCl Eutectic Melt. *Electrochim. Acta* **2009**, *54*, 4898-4902.
- (40) Evans, J.; Vincent, C. A.; Bruce, P. G. Electrochemical Measurement of Transference Numbers in Polymer Electrolytes. *Polymer* **1987**, *28*, 2324-2328.
- (41) Abraham, K. M.; Jiang, Z.; Carroll, B. Highly Conductive PEO-Like Polymer Electrolytes. *Chem. Mater.* **1997**, *9*, 1978-1988.
- (42) Seki, S.; Ohno, Y.; Miyashiro, H.; Kobayashi, Y.; Usami, A.; Mita, Y.; Terada, N.; Hayamizu, K.; Tsuzuki, S.; Watanabe, M. Quaternary Ammonium Room-Temperature Ionic Liquid/Lithium Salt Binary Electrolytes: Electrochemical Study. *J. Electrochem. Soc.* **2008**, *155*, A421-A427.